Role of Y in the oxidation resistance of CrAlYN coatings

S. Domínguez-Meister[a], S. El Mrabet[a], R. Escobar-Galindo[b], A. Mariscal[a], M.C. Jiménez de Haro[a], A. Justo[a], M. Brizuela[c], T.C. Rojas[a], J.C. Sánchez-López[a]

[a]Instituto de Ciencia de Materiales de Sevilla (CSIC-Univ. Sevilla), Avda. Américo Vespucio 49, 41092Sevilla, Spain

[b]Instituto de Ciencia de Materiales de Madrid (ICMM-CSIC), Sor Juana Inés de la Cruz 3, 28049 Cantoblanco, Spain

[c]TECNALIA, Mikeletegui Pasealekua, 2, 20009 Donostia-San Sebastián, Spain

Abstract

CrAlYN coatings with different aluminum (4 to 12 at.%) and yttrium (2 to 5 at.%) contents are deposited by d.c. reactive magnetron sputtering on silicon and M2 steel substrates using metallic targets and Ar/N_2 mixtures. The influence of the nanostructure and chemical elemental distribution on the oxidation resistance after heating in air at 1000ºC is studied by means of cross-sectional scanning electron microscopy (X-SEM), energy dispersive X-ray analysis (EDX), X-ray diffraction (XRD) and glow discharge optical emission spectroscopy (GD-OES). The sequential exposure to the metallic targets during the synthesis leads to a multilayer structure where concentration of metallic elements (Cr, Al and Y) is changing periodically. A good oxidation resistance is observed when Al- and Y-rich regions are separated by well-defined CrN layers, maintaining crystalline coherence along the columnar structure. This protective behavior is independent of the type of substrate and corresponds to the formation of a thin mixed (Al, Cr)-oxide scale that protects the film underneath. The GDOES and XRD analysis have demonstrated that Y acts as a reactive element, blocking the Fe and C atoms diffusion from the steel and favoring higher Al/Cr ratio in the passivation layer after heating. The coating with Y content around 4 at.% exhibited the best performance

with a thinner oxide scale, a delay in the CrN decomposition and transformation to Cr_2N, and a more effective Fe and C blocking.

Keywords: CrAlN; magnetron sputtering; Yttrium; oxidation resistance; mechanism

1. Introduction

$Cr_{1-x}Al_xN$ films deposited by physical vapor deposition have proven to be effective protective coatings for machining, casting, molding dies and sliding applications [1-7]. When exposed to air at elevated temperatures, $Cr_{1-x}Al_xN$ films form dense and adherent mixed aluminum and chromium oxide scales [1,8-9], which eventually suppress the oxygen diffusion into the bulk, providing excellent oxidation resistance up to temperatures as high as 900ºC [10-12], even at low Al content [13]. Current investigations seek to improve the thermal and oxidation resistance above this limit temperature by incorporation of large (substitutional) atoms, as they effectively retard diffusion related processes (recovery, decomposition and recrystallization). Yttrium has been proposed to be effective for this purpose by segregation to the oxide scale grain boundaries, blocking fast diffusion paths and increasing the onset for decomposition to 1100ºC [14-18]. Moreover, the addition of a reactive element was suggested to reduce the accumulation of voids at the substrate/scale interface [19] or to improve the mechanical properties of the scale by modifying the oxide scale structure [20]. Many of the reported works focus on coatings deposited on silicon substrates and the study of the thermal stability after annealing in vacuum. These investigations although necessary for characterizing the material properties are not appropriate to determine their capabilities and suitability as protective coating for steel tools and components exposed to air at high temperature. Moreover, although the benefits of incorporating yttrium seem to be proven little is known about the mechanisms of action of this rare earth element.

In a previous work, we demonstrated that yttrium (1.7 at.%) was better than zirconium to increase the oxidation resistance of CrAlN coatings deposited on silicon at 1000ºC in air with Al contents below 10 at. % [13], although zirconium was better to reduce friction [4]. Moreover, the protectiveness of nanostructured CrAlYN coatings [~4-12 at. % of Al; ~2-5 at.% of Y] deposited on P92 steel against steam oxidation at 650ºC was found to be comparable to conventional microstructured aluminides at much lower thickness than used for steam turbine components [21,22]. The influence of the location of the metallic elements inside ternary or quaternary nitrides and their chemical state may have a significant influence on the oxidation behavior and protective mechanism. The structure of these CrAlYN coatings was studied in detail with the help of advanced microscopic and analytical techniques with nanometric spatial resolution. A multilayer structure formed by alternating CrN and Cr-Al-Y-N layers was found as a result of the sequential exposure of the substrates to the material fluxes generated by the magnetron sources during rotation [23]. Depending on the target configuration, power applied to the magnetron and rotation speed, different film nanostructure and chemical composition were obtained. In this paper, these coatings are revised in terms of oxidation resistance, thermal and mechanical stability over coated M2 steels. The establishment of relationships between chemical and nanostructural features and their performance will be of high interest for their practical usage as protective coatings for advanced machining and high temperature applications.

2. Experimental

CrAlYN coatings with different Al and Y contents were deposited on Si (100) and M2 steel substrates using a commercial direct current (d.c.) magnetron sputtering equipment (CemeCon® CC800/8) provided with four rectangular targets (200 mm × 88 mm × 5 mm). The base pressure of the vacuum chamber was $\sim 1\times10^{-4}$ Pa and the working pressure set at 1 Pa from Ar/N_2 mixtures (ratio of 1.5). Two different target configurations (2Cr/1Al/1Y and

2Al/1Cr/1Y) and power applied to the yttrium target were used for controlling the chemical composition of the deposited films. Table 1 summarizes the applied Y-power, chemical composition, thickness and mechanical properties for the samples under investigation. A non-doped CrAlN coating was also prepared using two Cr and two Al targets as reference. The sputtering conditions were set to 3000 W for the chromium and aluminum targets. The yttrium target was fixed at two different sputtering powers: 1500W (samples A and C) and 3000W (samples B and D). The sample holder was negatively biased in the range of 110–120 V and the temperature ranged from 200 to 400 °C due to plasma heating effect. Full details about the synthesis conditions can be found in Ref. [23].

Chemical composition of the samples was obtained by electron probe microanalysis (EPMA) and glow discharge optical emission spectroscopy (GD-OES). The EPMA equipment was a JEOL JXA-8200 SuperProbe instrument equipped with four wavelengths detectors (WDS) and one energy-dispersive X-ray (EDX). GD-OES was used for obtaining the chemical depth profiling employing a Horiba Jobin Yvon RF instrument. This equipment was operated in argon plasma of 650 Pa and forward power of 40 W, with a 4 mm diameter copper anode. The wavelengths of the spectral lines used were 130.21 nm for oxygen, 149.26 nm for nitrogen, 371.99 nm for iron, 396.15 nm for aluminum, 425.23 nm for chromium and 371.03 nm for yttrium. The morphology and thickness of the coatings was investigated by preparing cross-section specimens and subsequent observation by scanning electron microscopy (SEM) in a high resolution FEG microscope, HITACHI-4800, equipped with an EDX detector (Bruker, XFlash4100), and transmission electron microscopy (TEM) in a Philips CM20 microscope operating at 200 kV. Cross-section views were obtained by cleaving silicon substrates, for SEM examination, and mechanical polishing followed by argon ion milling to electron transparency, in the case of TEM observation. The X-ray diffraction patterns were obtained in a Siemens D5000 diffractometer in the conventional θ–2θ Bragg-Brentano configuration and grazing angle incidence at 1 and 5º using Cu K_α

radiation. The mechanical properties were measured with a Fischerscope H100 dynamic microprobe instrument using a conventional Vickers indenter at loads up to 10 mN. The maximum load was selected in such a way that the maximum indentation depth did not exceed 10–15% of the coating thickness in order to avoid the influence of the substrate.

The oxidation experiments of all the coatings were performed in a furnace up to 1000 ºC at a heating rate of 10 °C/min and with a holding time of 2 h.

3. Results and discussion

3.1. Chemical and microstructural characterization

Table 1 summarizes the chemical composition obtained by EPMA, the thickness and hardness and Young's modulus values for the coatings. The hardness properties are found in the range of 24-30 GPa with H/E ratios close to 0.1. The aluminum contents increased from 4 to about 12 at.% when doubling the number of Al targets respectively. The increment of the Y content from 2 to 4-5 at.% is achieved by doubling the power from 1500 to 3000W. The nitrogen content remains almost constant at ~ 55 at.% and oxygen and carbon contaminants were less than 1 at.%.

The SEM cross-section images of the CrAlYN coatings are depicted in Figure 1. The CrAlYN-A and CrAlYN-B coatings present a typical columnar structure similar to that observed by the pure CrAlN in our previous publication [13]. The multilayer structure can be clearly seen in the inset images at higher magnification. The CrAlYN-C and CrAlYN-D coatings display a lesser columnar structure and a tile–mosaic can be observed in the insets, particularly at the highest Y power. All coatings present a multi-layered nanostructure as a consequence of the sequential exposure of the substrates to the different composition and disposition of the targets as we showed in our previous publication [23]. Figure 2 summarizes the most relevant results obtained together with a scheme of the target configuration used. In the CrAlYN-A and CrAlYN-B coatings (cf. Fig. 2, Set I), Al and Y-rich regions are

distributed in alternating layers that grow epitaxially on crystalline c-CrN layers. The presence of Al or Y inside the c-CrN regions forming ternary CrAlN or quaternary CrAlYN compounds cannot be discarded but their concentration appears more localized outside these c-CrN layers. For the CrAlYN-C and CrAlYN-D films, Al and Y atoms are mixed in the same region (central band in Fig. 2, Set II) forming an amorphous layer with some nanocrystals of c-(Cr)AlN and c-(Cr)YN embedded as demonstrated previously [23]. This amorphous Al-Y rich region appears separated by polycrystalline c-CrN layers. These differences can also be observed in the selected area diffraction (SAED) patterns. The SAED patterns agree well with highly oriented and crystalline c-Cr(Al,Y)N, in the first case, while rings with some spots are indicative of a polycrystalline nature in the second case. It is also worth mentioning that single or double thin layers of nanovoids filled with molecular nitrogen were also detected in the Y and Al rich regions [23].

The microcrystalline structure of the coatings was investigated by XRD in Bragg-Brentano configuration. Figure 3 shows the XRD scans of the as-deposited films on M2 steel substrates. The main peaks are in agreement with (111), (200) and (220) planes of cubic CrN phase (JCPDS 01-076-2494 - carlsbergite) although shifted to lower angles. This peak shift can be attributed to increasing residual stress and/or Y incorporation into the CrAlN lattice. The larger ionic radius of Y (106 pm) compared to Cr (64 pm) and Al (57 pm) results in a lattice expansion. However, the increment of the Al content in the C and D samples reduces this peak shifting owing to a decrease of the interplanar spacing when Al atoms, of lower radius, substitute Cr atoms in the cubic cell. The preferred orientations are observed to be <111> and <220> in CrAlN and <200> for CrAlYN samples. The CrAlN presents a hardness of 30 GPa while the Y-doped samples exhibit slight lower values (24 to 28 GPa). The elastic moduli change in the same direction giving H/E ratios of 0.10 and 0.13 for CrAlN and CrAlYN coatings respectively.

3.2. Oxidation resistance

3.2.1. Coatings deposited on silicon substrates

Figure 4 illustrates representative SEM cross–sections images of the coatings A and C grown on silicon and their associated EDX spectra obtained after oxidation at 1000ºC for 2 h in air. The inner structure of CrAlYN-A coating remains comparable after heating and a thin oxide surface layer is developed. The EDX spectrum shown in Fig. 4b corroborates the oxide nature of this scale. The increase of oxygen and aluminum peaks is indicating the outwards diffusion of aluminum forming a mixed (Cr,Al)-oxide scale. The EDX spectrum measured inside shows still the presence of Cr and N revealing a good thermal stability. However, a similar treatment carried out with the CrAlYN-C coating did not yield comparable results. The SEM image shown in Fig. 4c revealed a drastic change of initial film morphology towards a granular and porous structure. This transformation seems to be in agreement with a full oxidation of the coating as lately confirmed by EDX (cf. Fig. 4d). The comparison between the initial and annealed spectrum indicates the significant increment of O and Al signals while N is almost disappearing. The increment of the silicon peak put in evidence the diffusion of silicon from the substrate promoted by heating. The different oxidation behavior can be correlated with the differences in nanostructure and chemical composition obtained for set I and II; however, the nature of the substrate has also to be considered. The diffusion of metallic elements from the substrate to the surface during oxidation and thermal treatment is an important phenomenon that influences certainly the protectiveness and barrier layer effect of the developed coating. This point is commonly disregarded in many papers and results of primary importance as to determine the practical performance in industrial applications. By this reason, we further proceeded to investigate the results with coated steel specimens.

3.2.2. Coating deposited on M2 steels

In order to study the oxidation behavior of the coatings deposited onto M2 steel a XRD analysis in standard Bragg-Brentano configuration was carried out on the samples heated at 1000ºC for 2 h in air. Figure 5 displays the XRD diffractograms for the four CrAlYN and the CrAlN reference including labels for the main identified phases. The first conclusion is that only in two cases (CrAlYN-A and B) the initial peaks of cubic CrN phase are still present although their intensities are decreased owing to the transformation to hexagonal Cr_2N. As observed in the initial state, these peaks are shifted toward lower angles as a consequence of internal stresses and/or yttrium alloying. The CrAlYN-C, and particularly the CrAlYN-D, coatings show evidences of h-Cr_2N, as can be noticed by the (111) peak around 42.6º, although accompanied by numerous peaks from chromium, aluminum and iron oxide phases. Finally, the worst performance is obtained with the CrAlN reference where no evidences of chromium nitride phases (CrN or Cr_2N) are found, being transformed to Cr_2O_3. In these three cases, the outward diffusion of metals and carbon from the coating and the M2 steel, together with the inwards diffusion of oxygen are the responsible of the formation of Cr_2O_3, Al_2O_3, Cr_7C_3, Fe_3O_4 and Fe_2O_3 phases.

This assembly of results is proving the direct influence of the type of substrate on the oxidation mechanism and products generated. Thus, the oxidation progresses to a major extent for highly corrodible substrate as M2 versus silicon (more passive element and even beneficial for thermal stability by alloying with the transition metal nitride). This conclusion is worth of consideration since many papers have reported oxidation resistance of CrAlN-based compounds showing outstanding performance even up to temperatures of 1400ºC but deposited on silicon pieces so the results cannot be extrapolated straightforwardly for functional applications on steel [14,15].

The incorporation of yttrium in CrAlYN-A and CrAlYN-B led to a significant improvement in comparison to the non-doped CrAlN sample. These three samples were then selected for a deeper study by measuring the XRD scans in θ-2θº configuration and at grazing

angles of 1 and 5º. Under these conditions it is possible to obtain information about the phase composition from the oxidation topmost layer and inner regions.

Figure 6 presents the zoomed region (30 to 50º) at increasing incidence angles for CrAlN, CrAlYN-A and CrAlYN-B films. The CrAlN coating manifests clear evidences of film degradation as the main peak related to cubic CrN phase is disappearing and chromium and iron oxides are formed, especially in the surface. The formation of chromium carbide (Cr_7C_3) is also noticed in the vicinity of the steel interface. This corrosion product appears by the reaction of carbon atoms diffusing from the substrate with the chromium formerly forming part of the metallic nitride. Moreover, a progressive enrichment in α-Fe_2O_3 (hematite) in the surface indicating a fast diffusion of iron from the substrate. In the yttrium-containing samples (CrAlYN-A and CrAlYN-B), only Cr_2O_3 is detected preferentially in the surface whilst the presence of hexagonal Cr_2N and cubic CrN chromium nitride phases is observed inside the coatings. The positions of these peaks are shifted towards lower angles in both cases and attributed to residual compressive stresses in these phases generated during thermal annealing and possible incorporation of metallic ions from the steel. The formation of h-Cr_2N comes from the decomposition of the CrN and the release of nitrogen as observed by us and other authors [13-15]. The maximum intensity of the peak (111) of Cr_2N is observed in the region closer to the steel substrate where the diffusion of elements from the substrate promotes the CrN decomposition. The formation of Cr_7C_3 and Fe_2O_3 is observed to decrease with the yttrium content whose peaks are less intense or absent. As a general comment, no aluminum oxides are detected by XRD in these set of coatings. These oxides are probably not detected due to the low Al content in these coatings being amorphous or mixed with Cr_2O_3 since the quasibinary Al_2O_3- Cr_2O_3 shows complete miscibility [3,25]. Focusing on the XRD-scan measured at 5º, which contains information from the top oxide layer and the inner film, and comparing the relative intensities of the oxide and c-CrN phases it can be concluded that a higher proportion of CrN is obtained in the CrAlYN-B film where the yttrium content was

higher (close to 4 at.%). This is indicative of a better oxidation resistance of this coating when submitted to oxidation at 1000ºC during 2 hours. A different behavior has been reported recently by Qi et al. [3] where the best performance of CrAlYN coatings was obtained for Y contents below 1 at. %. Rovere et al. [14,15] reported that coatings with 2 and 4 mol% YN (1 and 2 at.% of Y) exhibited lower weight gains during exothermal oxidation. An explanation of these differences in the limit of Y incorporation can be attributed to a different nanostructure and chemical composition of the coatings in respect to the coatings here presented. Those works report $Cr_{1-x}Al_xN$ coatings with $x \geq 0.5$ (i.e. Al contents > 20-25 at. %) higher than the values presented here. In addition, the multi-layered structure with periodic alternating chemical composition supposes an additional parameter to be considered and therefore a different oxidation mechanism can be foreseen [26].

With the aim of further studying the influence of the yttrium content and its role in the oxidation resistance, a depth profiling chemical analysis was carried out on the oxidized samples by GDOES. Fig. 7 displays the chemical compositions after oxidation at 1000ºC for the CrAlN, CrAlYN-A and B coatings deposited on M2 steel. A significant depletion in N content is observed inside the CrAlN coating, indicative of the nitrogen removal by decomposition of the CrN during the treatment. The superficial region is enriched in chromium, iron and oxygen in agreement with the Cr_2O_3, Fe_3O_4 and Fe_2O_3 phases identified by XRD analysis. The oxygen signal is essentially limited to this surface layer and no noticeable inward oxygen diffusion is observed beyond 1μm thickness. The Al amount is almost constant along the inner region with a slight enrichment in the oxide/film interface. An important result is the outward diffusion of Fe and C atoms from the steel across the coating during heating treatment. Due to the greater affinity of the Cr towards the carbon atoms, the Cr_7C_3 phase is formed inside, while the Fe atoms combine with oxygen to form Fe_3O_4 and Fe_2O_3 in the surface.

In the case of Y-doped CrAlN coatings a thinner oxide scale is observed (around 250 nm), a delay of the CrN decomposition and nitrogen removal. The Al signal is almost constant along the film thickness but Cr decreases substantially in the oxide surface layer meaning a higher Al/Cr ratio in the passivation layer as compared to the non-doped sample. Likewise, yttrium signal diminished in the top surface but appears slightly higher in the film/steel interface. The oxygen signal drops significantly after passing through the passivation layer and steadies around 6-7 at.% in CrAlYN-B. This value remains stable until reaching the film/substrate interface in contrast to CrAlN and CrAlYN-A where it vanished to zero around 1 μm. The incorporation of yttrium in the film composition appears to retard the diffusion of elements from the steel substrate, particularly at the highest content (3.7 at.%) – CrAlYN-B. There is a correlation between the limited oxygen penetration, the blocking of Fe/C elements from the substrate and the presence of yttrium. Yttrium is reported to inhibit the cation diffusion along the grain boundaries [27] affecting the release of elements from the substrate.

Discussion

These results shed light on the role of yttrium as a reactive element in the protectiveness of these metallic nitrides coatings against oxidation. The observed effects are the retard of the CrN decomposition, the formation of a mixed Cr-Al oxide passivation layer, the controlled inward oxygen and outward (iron and carbon) diffusion. Furthermore, the chemical distribution and bonding type in the quaternary CrAlYN compounds has definitively an influence on the protectiveness behavior. The samples grown with 2 Al targets (Set II) showed a worse protective behavior with different oxidation mechanism and corrosion products that is correlated to the initial differences in chemical and structural features. Under this target configuration a multilayer structure was obtained where amorphous (Al/Y-rich) and crystalline (Cr-rich) nitride regions were alternating. However, in the first set of coatings (Set I), Al and Y-rich layers were separated by fcc-CrN layers and Al/Y atoms are substitutional

atoms in the CrN lattice. This situation allows a continuous homoepitaxial growth of crystalline c-CrN where Al or Y atoms are periodically incorporated. As a consequence, the internal stresses produced by different expansion coefficients between layers under heating are lower in this case as there is no lattice mismatch. The inter-diffusion at the interfaces and the oxygen attacks greatly influence the thermal stability and oxidation resistance at elevated temperatures [28]. In addition, the tile mosaic structure observed in the CrAlYN-C and CrAlYN-D increases the number of pathways for fast ion diffusion (metal outwards and oxygen inwards). Both combined effects justified the worse performance as mechanical stability and oxidation resistance are seriously limited.

Consequently, yttrium retards the CrN decomposition to Cr_2N and nitrogen removal. The role of yttrium in the oxidation mechanism appears to be connected with the ion transport across the film. In the surface, a passivation layer rich in Cr and Al oxides is formed together with small amounts of iron oxides, as stated by grazing incidence XRD. The Al/Cr ratio is enhanced in the passivation layer as compared to the samples without yttrium. Inside, oxygen inlet is limited up to 6-7 at.% and should be associated to Al and Y atoms removed from the cubic Cr(Al/Y)N phases. These aluminum and yttrium oxides have to be amorphous since they could not be detected by XRD or are mixed with Cr_2O_3 forming alloys. The fact that relative diffusion rates between oxygen (inward) and cations (outward) is affected by the presence of yttrium leads to a limited oxygen incorporation (stable and below 7 at.%) and the blockage of Fe and C diffusion from the steel substrate. The formation of aluminum and yttrium oxides at the grain boundaries would serve to seal the pathways for Fe propagation. Iron atoms diffusing from the substrate are immediately oxidized at the film/substrate interface stopping their propagation to the surface. We are currently undergoing further studies to visualize the ion diffusion, phase formation and spatial distribution in order to fully understand the oxidation mechanism with the help of advanced analytical transmission electron microscopy on coatings deposited on steels. Other influencing parameters to be

investigated are the increment in aluminum contents and the multilayer architecture vs. a nanocomposite whereas all the phases are distributed randomly. These studies will be the object of future publications.

Conclusions

The oxidation resistance of CrAlYN-based coatings prepared by magnetron sputtering with different nanostructure and metal distribution has been studied comparatively using different type of substrates (silicon and M2 steel). The addition of ~ 4 at.% of yttrium was demonstrated to enhance the oxidation resistance up to 1000ºC for low aluminum contents (<10 at.%). Thus, the beneficial effect of aluminum as protective agent of CrN phases against oxygen reactivity is reinforced in the case of yttrium by reducing the corrosion products and modifying the oxide growth mechanism. The increased Al/Cr ratio in the surface passivation layer and controlled oxygen diffusion inwards affects positively the film oxidation resistance. Mixed Al-Y oxides formed inside the coating appear to block the diffusion of elements from the substrate, preventing the CrAlYN decomposition and oxidation.

Acknowledgments

The authors are grateful to the Spanish Ministry of Science and Innovation (projects No. MAT2007-66881, MAT2010-21597, MAT2011-29074 and Consolider FUNCOAT CSD2008-00023), Junta de Andalucía (TEP217) and I3P programme of CSIC for financial support.

References

1. O. Banakh, P. E. Schmid, R. Sanjines, E. Levy, High-temperature oxidation resistance of $Cr_{1-x}Al_xN$ thin films deposited by reactive magnetron sputtering, Surf. Coat. Technol. 163 (2003) 57-61.
2. A. E. Reiter, V. H. Derflinger, B. Hanselmann, T. Bachmann, B. Sartory, Investigation of the properties of $Al_{1-x}Cr_xN$ coatings prepared by cathodic arc evaporation, Surf. Coat. Technol. 200 (2005) 2114-2122.
3. Z. T. Qi, Z. T. Wu, Z. C. Wang, Improved hardness and oxidation resistance for CrAlN hard coatings with Y addition by magnetron co-sputtering, Surf. Coat. Technol.259 (2014) 146-151.
4. J. C. Sanchez-Lopez, A. Contreras, S. Dominguez-Meister, A. Garcia-Luis, M. Brizuela, Tribological behaviour at high temperature of hard CrAlN coatings doped with Y or Zr, Thin Solid Films 550 (2014) 413-420.
5. M. Brizuela, A. Garcia-Luis, I. Braceras, J. I. Onate, J. C. Sanchez-Lopez, D. Martinez-Martinez, C. Lopez-Cartes, A. Fernandez, Magnetron sputtering of Cr(AI)N coatings: Mechanical and tribological study, Surf. Coat. Technol. 200 (2005) 192-197.
6. H. C. Barshilia, N. Selvakumar, B. Deepthi, K. S. Rajam, A comparative study of reactive direct current magnetron sputtered CrAlN and CrN coatings, Surf. Coat. Technol. 201(2006) 2193-2201.
7. J. Lin, B. Mishra, J. J. Moore, W. D. Sproul, Microstructure, mechanical and tribological properties of $Cr_{1-x}Al_xN$ films deposited by pulsed-closed field unbalanced magnetron sputtering (P-CFUBMS), Surf. Coat. Technol. 201 (2006) 4329-4334.
8. J. Endrino, G. S. Fox-Rabinovich, A. Reiter, S. V. Veldhuis, R. E. Galindo, J. M. Albella, J. F. Marco, Oxidation tuning in AlCrN coatings, Surf. Coat. Technol. 201 (2007) 4505-4511.

9. R. Escobar Galindo, J. L. Endrino, R. Martinez, J. M. Albella, Improving the oxidation resistance of AlCrN coatings by tailoring chromium out-diffusion, Spectrochimica Acta Part B 65 (2010) 950-958.
10. M. Kawate, A. K. Hashimoto, T. Suzuki, Oxidation resistance of $Cr_{1-x}Al_xN$ and $Ti_{1-x}Al_xN$ films, Surf. Coat. Technol. 165(2) (2003) 163-167.
11. H. Willmann, P. H. Mayrhofer, P. O. A. Persson, A. E. Reiter, L. Hultman, C. Mitterer, Thermal stability of Al-Cr-N hard coatings, Scripta Mater. 54 (2006) 1847-1851.
12. H. C. Barshilia, B. Deepthi, K. S. Rajam, K. P. Bhatti, S. Chaudhary, Growth and characterization of TiAlN/CrAlN superlattices prepared by reactive direct current magnetron sputtering, J. Vac. Sci. Technol. A 27 (2009) 29-36.
13. T. C. Rojas, S. El Mrabet, S. Dominguez-Meister, M. Brizuela, A. Garcia-Luis, J. C. Sanchez-Lopez, Chemical and microstructural characterization of (Y or Zr)-doped CrAlN coatings, Surf. Coat. Technol. 211 (2012) 104-110.
14. F. Rovere, P. H. Mayrhofer, A. Reinholdt, J. Mayer, J. M. Schneider, The effect of yttrium incorporation on the oxidation resistance of Cr-Al-N coatings, Surf. Coat. Technol. 202 (2008) 5870-5875.
15. F. Rovere, P. H. Mayrhofer, Thermal stability and thermo-mechanical properties of magnetron sputtered Cr-Al-Y-N coatings, J. Vac. Sci. Technol. A 26 (2008) 29-35.
16. K. D. Bouzakis, N. Michailidis, S. Gerardis, G. Katirtzoglou, E. Lili, M. Pappa, M. Brizuela, A. Garcia-Luis, R. Cremer, Correlation of the impact resistance of variously doped CrAlN PVD coatings with their cutting performance in milling aerospace alloys, Surf. Coat. Technol. 203 (2008) 781-785.
17. F. Rovere, D. Music, J. M. Schneider, P. H. Mayrhofer, Experimental and computational study on the effect of yttrium on the phase stability of sputtered Cr-Al-Y-N hard coatings, Acta Mater. 58 (2010) 2708-2715.

18. R. Braun, F. Rovere, P. H. Mayrhofer, C. Leyens, Environmental protection of gamma-TiAl based alloy Ti-45Al-8Nb by CrAlYN thin films and thermal barrier coatings, Intermetallics 18 (2010) 479-486.
19. D. P. Whittle, J. Stringer, Improvements in high-temperature oxidation resistance by additions of reactive elements or oxide dispersions, Philos. Trans. R. Soc. London Ser. A-Math. Phys. Eng. Sci. 295(1413) (1980) 309-329.
20. F. J. Perez, S. I. Castaneda, M. P. Hierro, R. E. Galindo, J. C. Sanchez-Lopez, S. Mato, Comparative Study of Micro- and Nano-structured Coatings for High-Temperature Oxidation in Steam Atmospheres, Oxidation of Metals 81(2014) 227-236.
21. S. Mato, G. Alcala, M. Brizuela, R. E. Galindo, F. J. Perez, J. C. Sanchez-Lopez, Long-term high temperature oxidation of CrAl(Y)N coatings in steam atmosphere, Corr. Sci. 80 (2014) 453-460.
22. Y. Saito, T. Maruyama, T. Amano, Adherence of oxide scale forme don Ni-20Cr-1Si alloys with small additions of rare-earth elements, Mater. Sci. Eng. 87 (1987) 275-280.
23. T. C. Rojas, S. Dominguez-Meister, M. Brizuela, A. Garcia-Luis, A. Fernandez, J. C. Sanchez-Lopez, A Nanoscale Characterization with Electron Microscopy of Multilayered CrAlYN Coatings: A Singular Functional Nanostructure, Microsc. Mycroanal. 20 (2014) 14-24.
24. J. L. Chen, C. X. Guo, J. Chen, J. J. He, Y. J. Ren, L. L. Hu, Microstructure, optical and electrical properties of CrAlN film as a novel material for high temperature solar selective absorber applications, Mater. Lett. 133 (2014) 71-74.
25. S.S. Kim, T.H. Sanders, J. Am. Ceram. Soc. 84 (2001) 1881-1884.
26. N. Fukumoto, H. Ezura, T. Suzuki, Synthesis and oxidation resistance of TiAlSiN and multilayer TiAlSiN/CrAlN coating. Surf. Coat. Technol. 204 (2009) 902-906.

27. R. Prescott, M. J. Graham, The formation of aluminum-oxide scales on high-temperature alloys, Oxidation of Metals 38 (1992) 233-254.
28. S.K. Tien, C.H. Lin, Y.Z. Tsai, J.G. Duh, Oxidation behaviour, microstructure evolution and thermal stability in nanostructured CrN/AlN multilayer hard coatings.

Figure captions

1. Cross-section SEM images of the as-deposited CrAlYN coatings on silicon substrates from CrAlYN-A (a), CrAlYN-B (b), CrAlYN-C (c), CrAlYN-D (d). Details at higher magnification are shown as insets.
2. Representative X-TEM images corresponding to set I (CrAlYN-A) and II (CrAlYN-C) coatings. The phase composition is depicted schematically in the same figure together with the target distribution employed in the PVD chamber for their synthesis.
3. XRD diffractograms of the CrAlYN and CrAlN coatings as-deposited onto M2 steels (θ-2θº configuration). CrN (JCPDS card# 01-076-2494) and steel substrate XRD positions are marked for comparison.
4. SEM cross-section pictures of CrAlYN-A (a), CrAlYN-C (c) coatings deposited onto silicon and associated EDX analysis (c and d, respectively) made after oxidation in air at 1000ºC.
5. XRD diffractograms of the CrAlYN and CrAlN coatings deposited onto M2 steels after oxidation in air at 1000ºC measured in θ-2θº. JCPDS card numbers: CrN (01-076-2494); Cr_2N (35-0803); Cr_2O_3-a (38-1479); Cr_2O_3-b (1-84-0315); Cr_7C_3 (36-1482); Al_2O_3 (1-75-0785); Fe_3O_4 (19-0629); Fe_2O_3 (33-0664); Fe (1-87-721).
6. XRD diffractograms of the CrAlN, CrAlYN-A and CrAlYN-B coatings deposited onto M2 steels after oxidation in air at 1000ºC measured in θ-2θº and grazing angle configuration at 1 and 5º. JCPDS card numbers: CrN (01-076-2494); Cr_2N (35-0803); Cr_2O_3-a (38-1479); Cr_2O_3-b (1-84-0315); Cr_7C_3 (36-1482); Al_2O_3 (1-75-0785); Fe_3O_4 (19-0629); Fe_2O_3 (33-0664); Fe (1-87-721).
7. GDOES spectra of coatings CrAlN, CrAlYN-A and CrAlYN-B coatings measured oxidation in air at 1000ºC.

Table 1. Chemical composition, thickness and tribo-mechanical properties of the CrAl(Y)N coatings.

Sample		Power Y	Cr	Al	Y	N	thickness	H	E
		W	at.%				μm	GPa	GPa
CrAlYN-A	Set I	1500	40.1	4.0	1.6	54.3	3.8	24	187
CrAlYN-B		3000	39.3	3.6	3.7	53.4	4.5	28	210
CrAlYN-C	Set II	1500	32.7	11.8	2.2	53.4	3.0	25	187
CrAlYN-D		3000	31.5	11.5	5.0	52	2.1	26	199
CrAlN	Reference	-	36.5	8.3	-	55.2	3.3	30	304

Table 1. Chemical composition, thickness and tribo-mechanical properties of the CrAl(Y)N coatings.

Sample		Power Y	Cr	Al	Y	N	thickness	H	E
		W	at.%				μm	GPa	GPa
CrAlYN-A	Set I	1500	40.1	4.0	1.6	54.3	3.8	24	187
CrAlYN-B		3000	39.3	3.6	3.7	53.4	4.5	28	210
CrAlYN-C	Set II	1500	32.7	11.8	2.2	53.4	3.0	25	187
CrAlYN-D		3000	31.5	11.5	5.0	52	2.1	26	199
CrAlN	Reference	-	36.5	8.3	-	55.2	3.3	30	304

Figure

Click here to download high resolution image

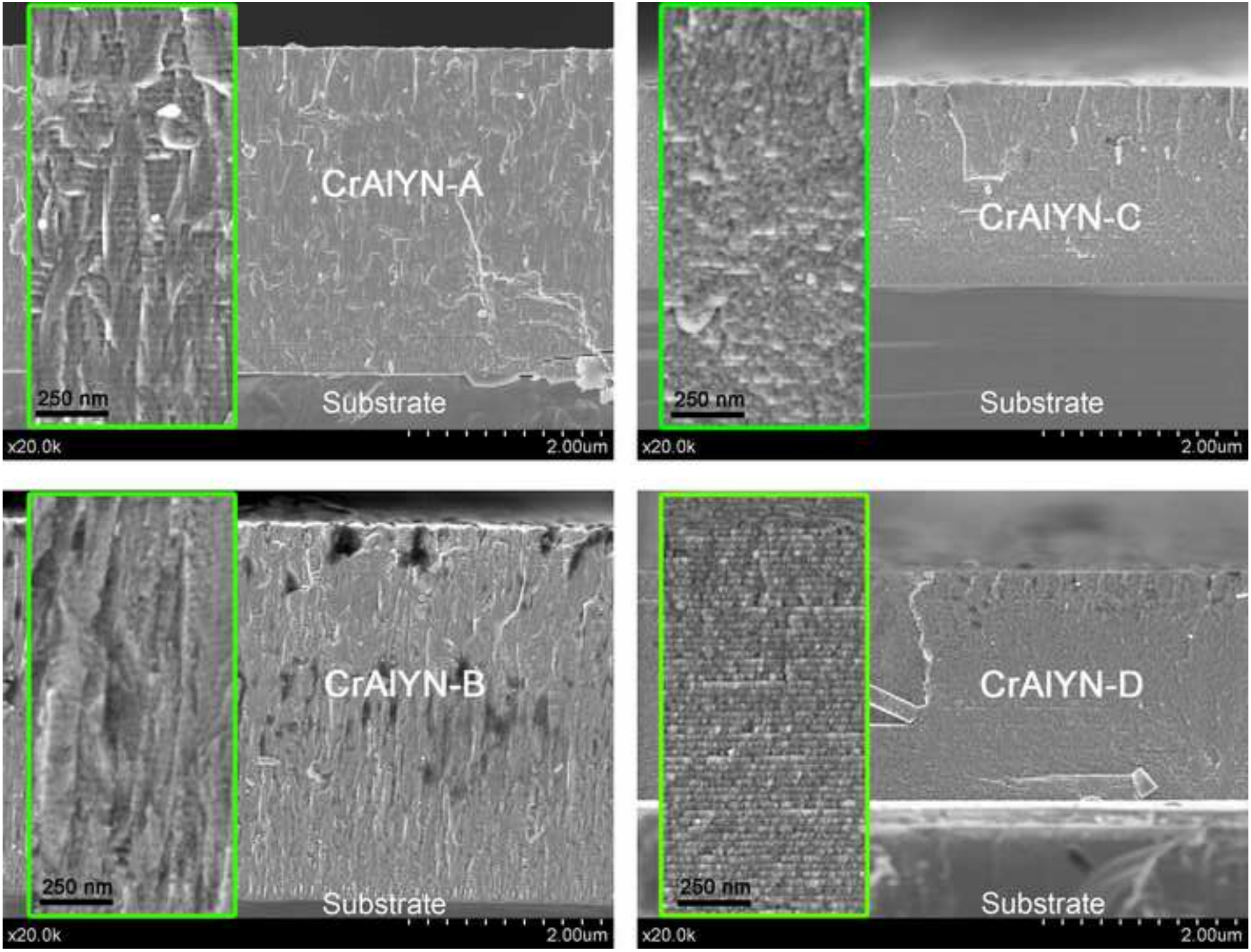

Figure 2

Click here to download high resolution image

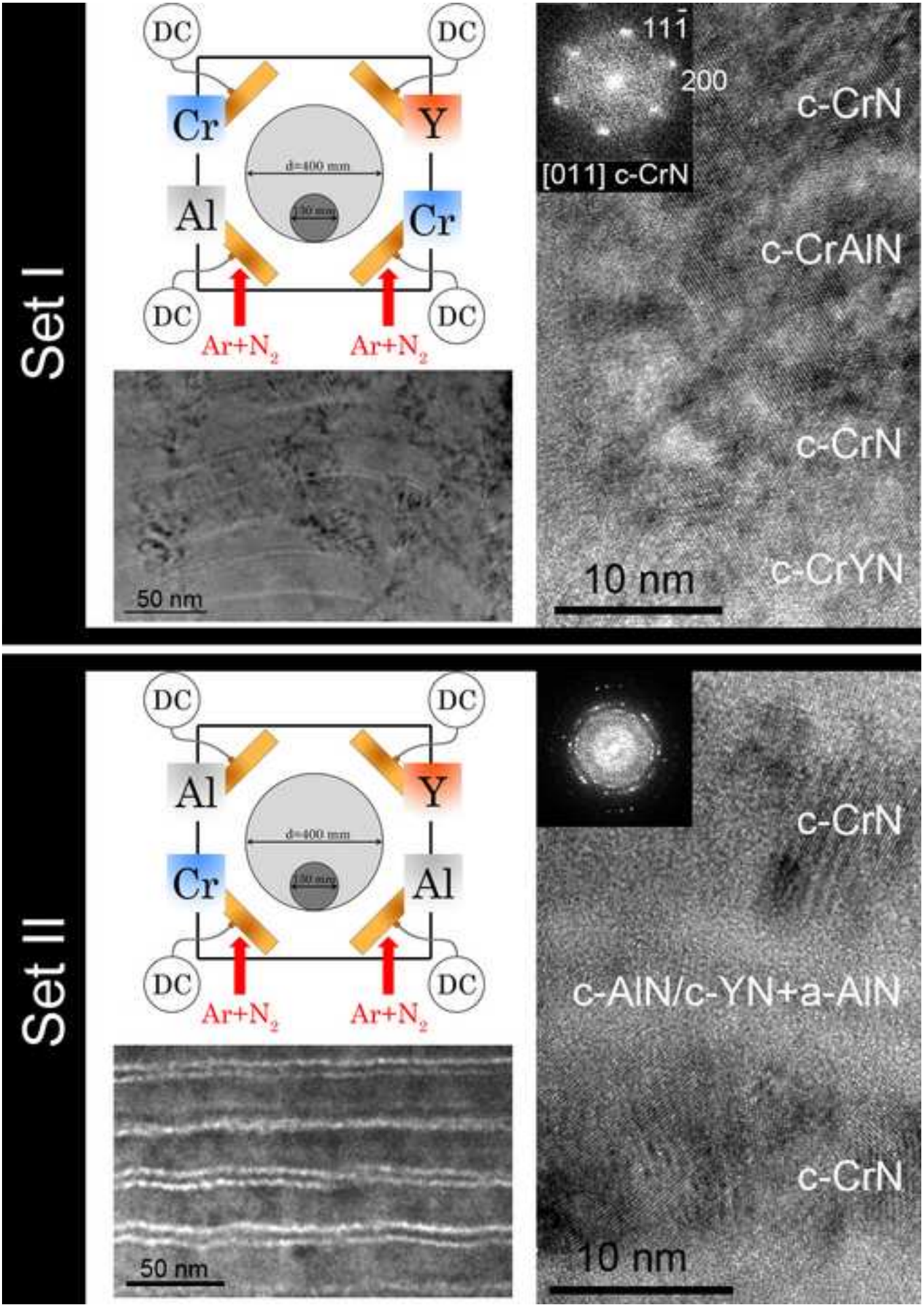

Figure 3

Click here to download high resolution image

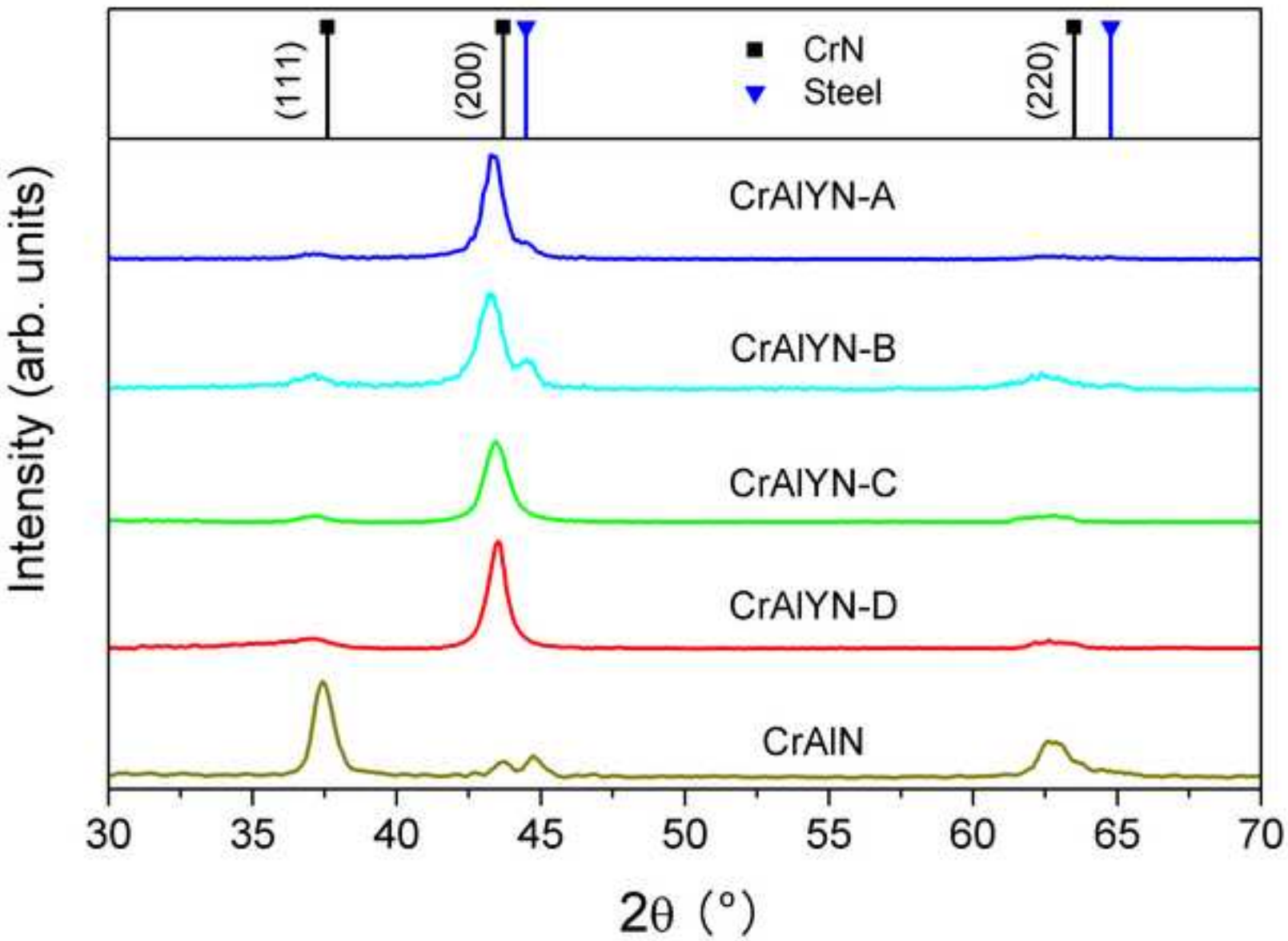

Figure 4

Click here to download high resolution image

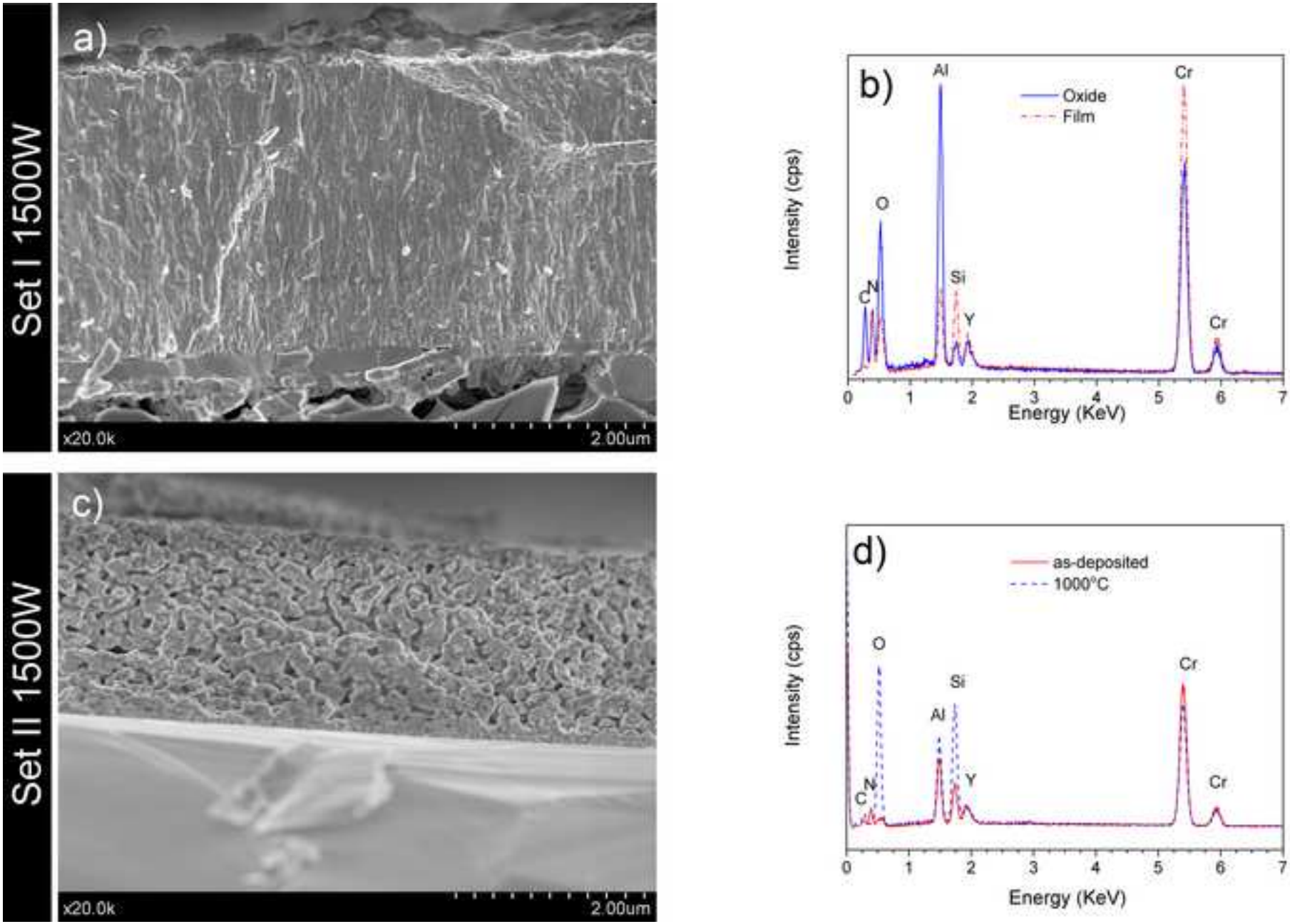

Figure 5

Click here to download high resolution image

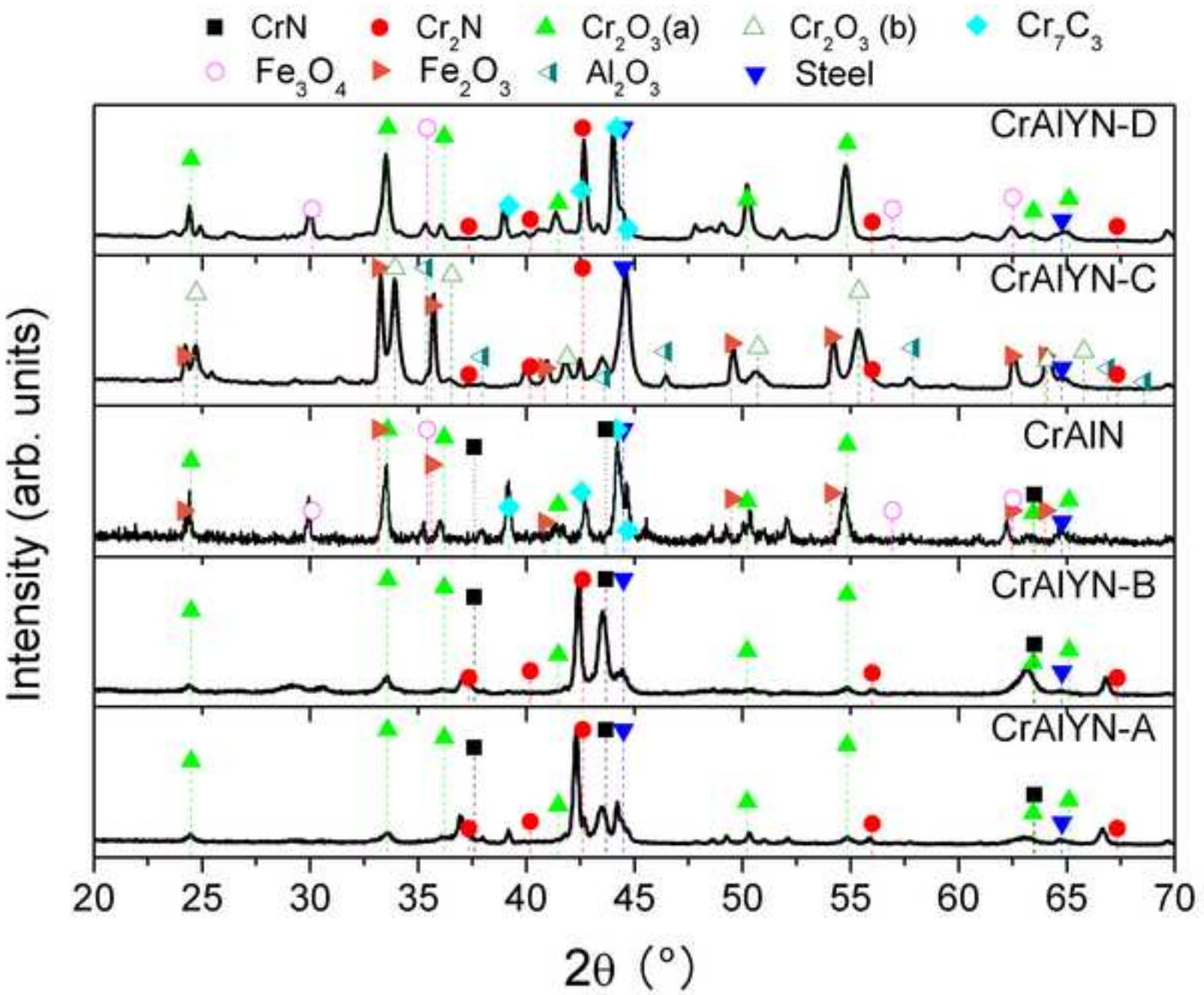

Figure 6a

Click here to download high resolution image

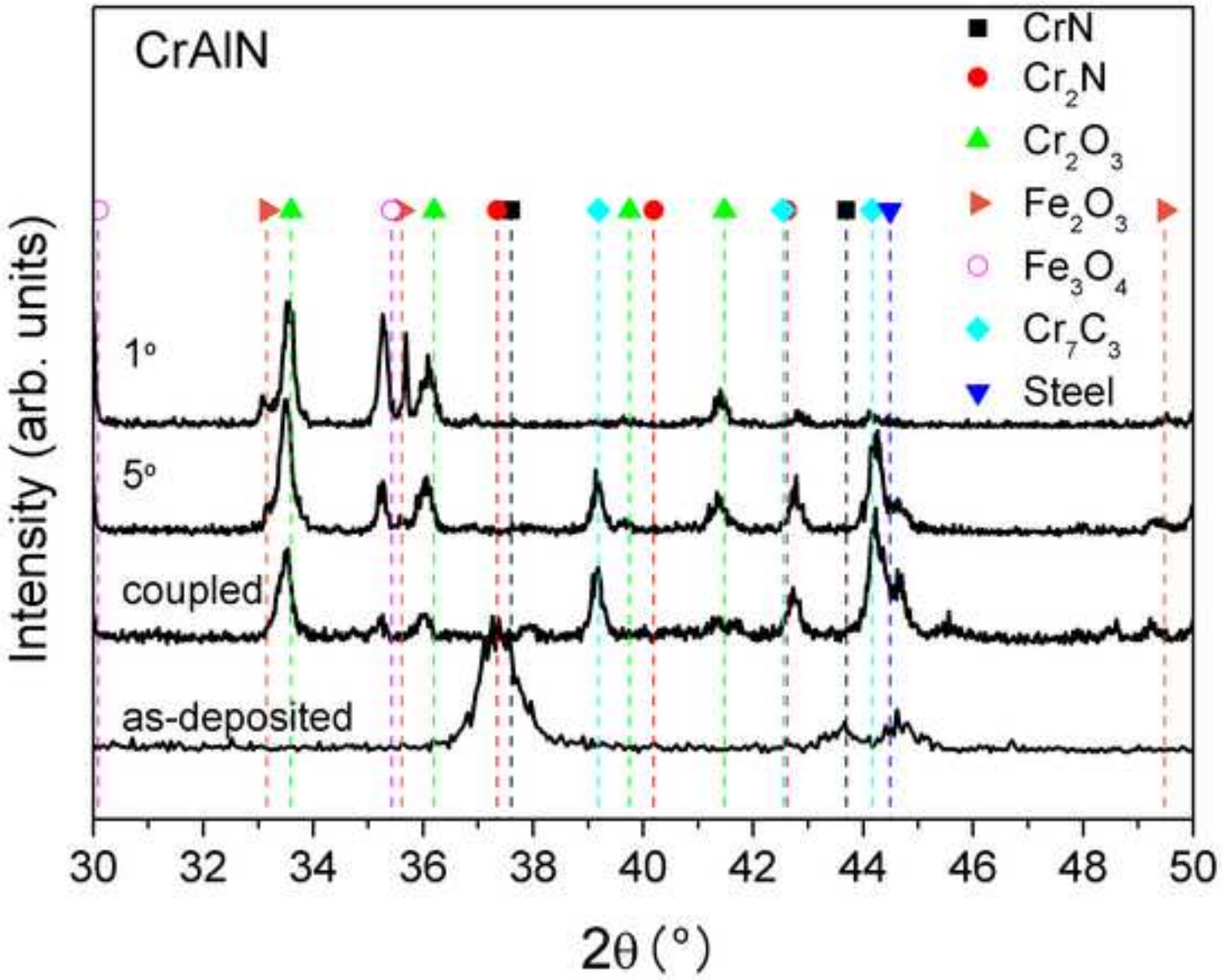

Figure 6b

Click here to download high resolution image

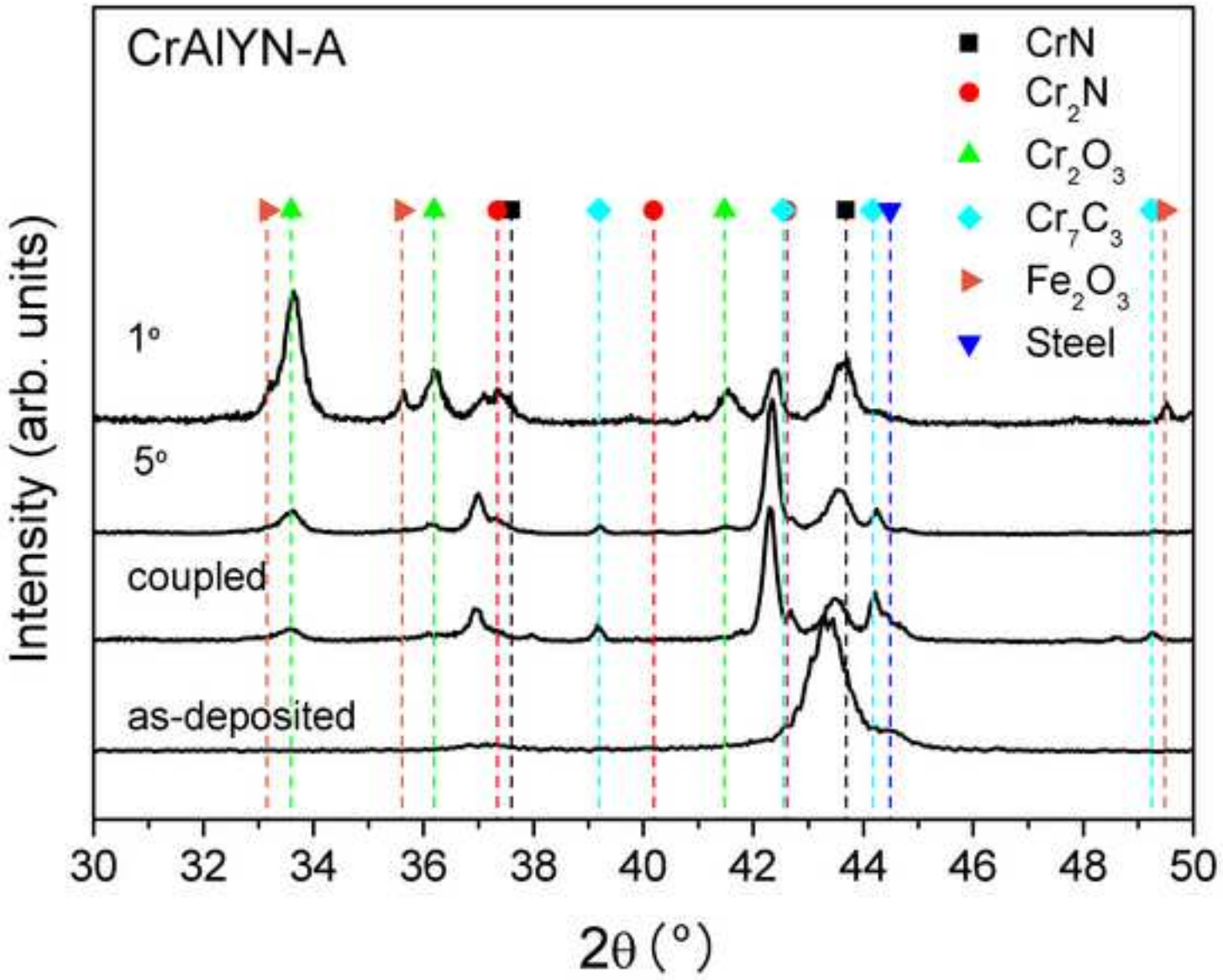

Figure 6c

Click here to download high resolution image

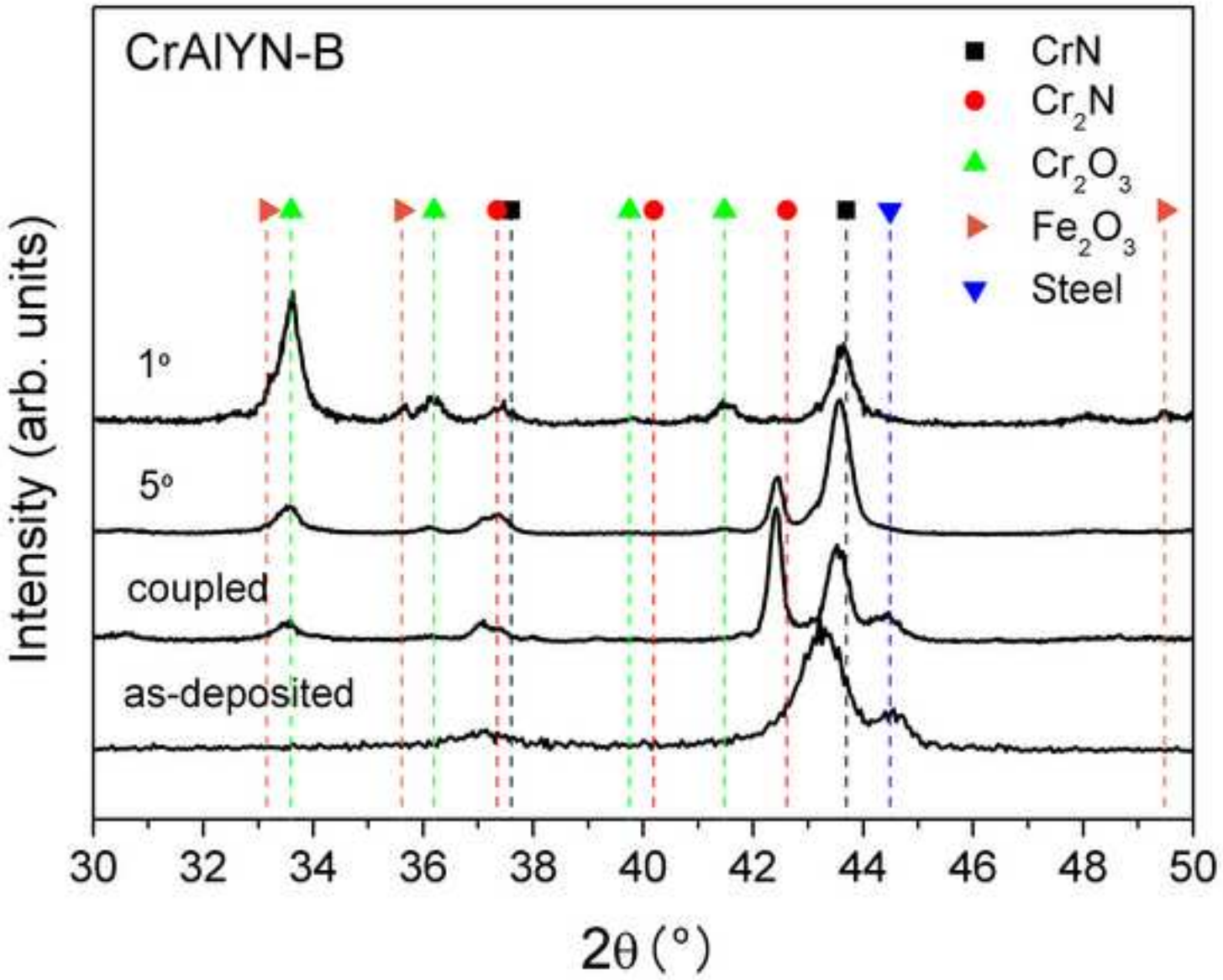

Figure 7

Click here to download high resolution image

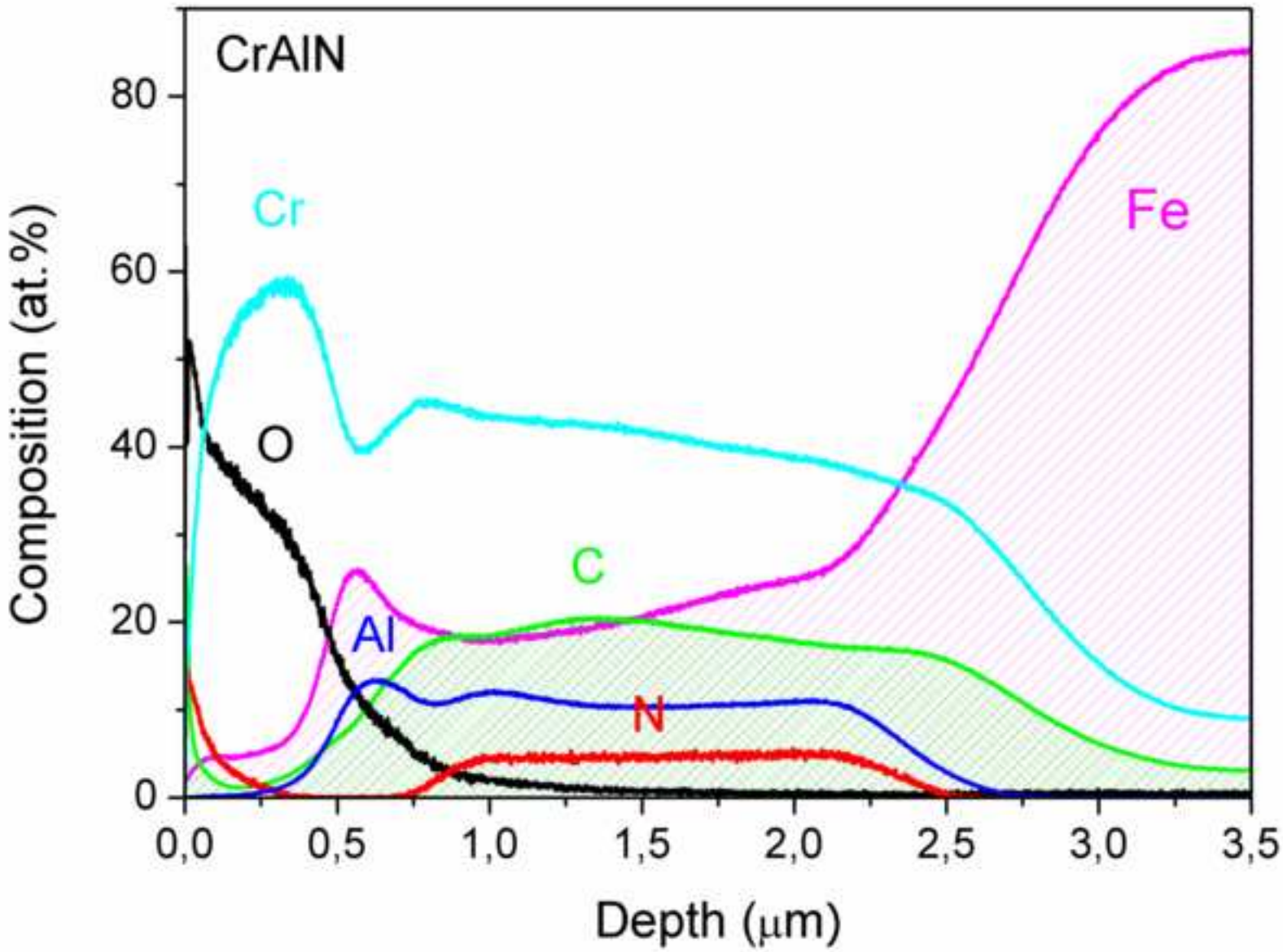

Figure 7 (2)
Click here to download high resolution image

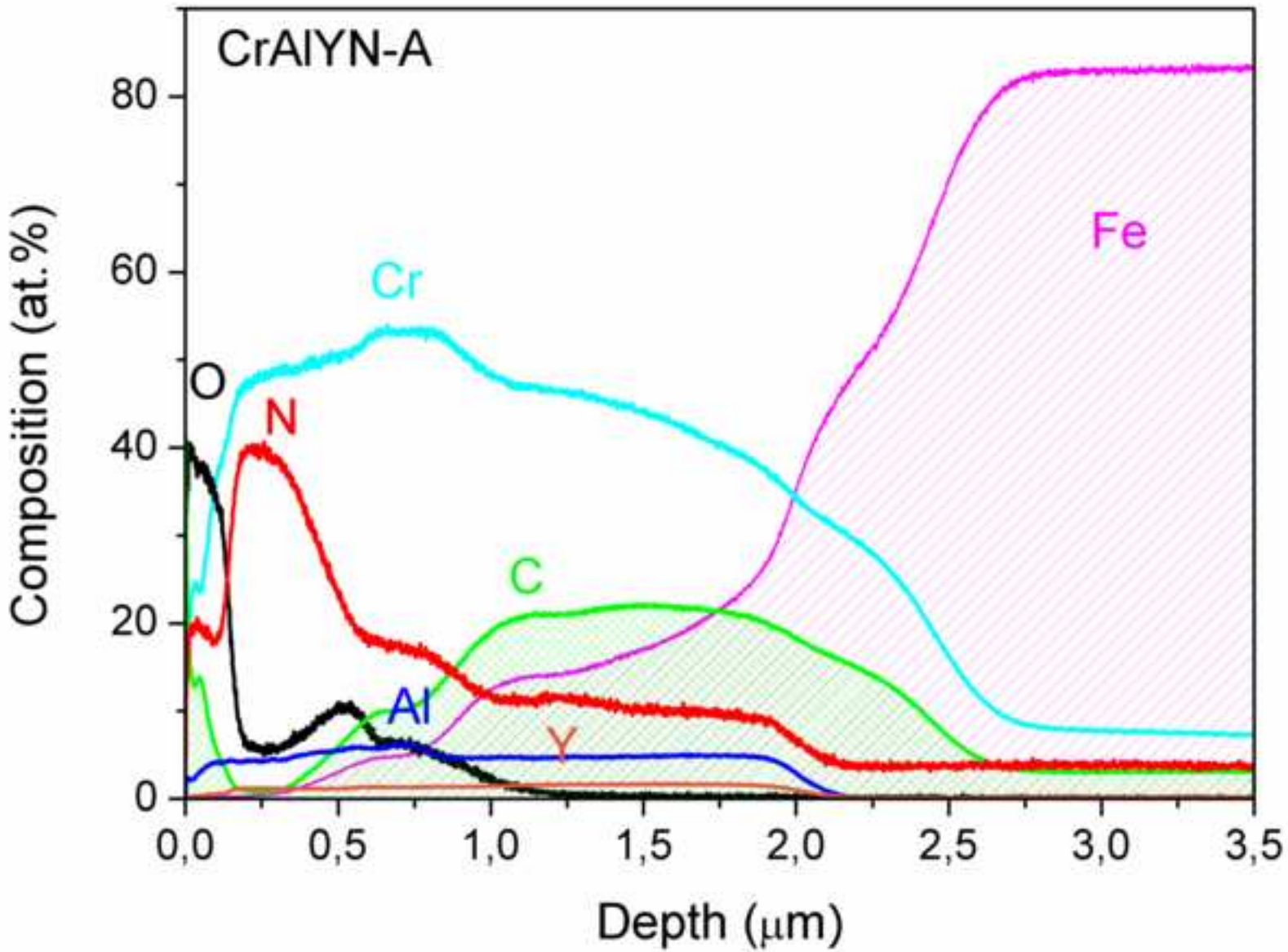

Figure 7 (3)
Click here to download high resolution image

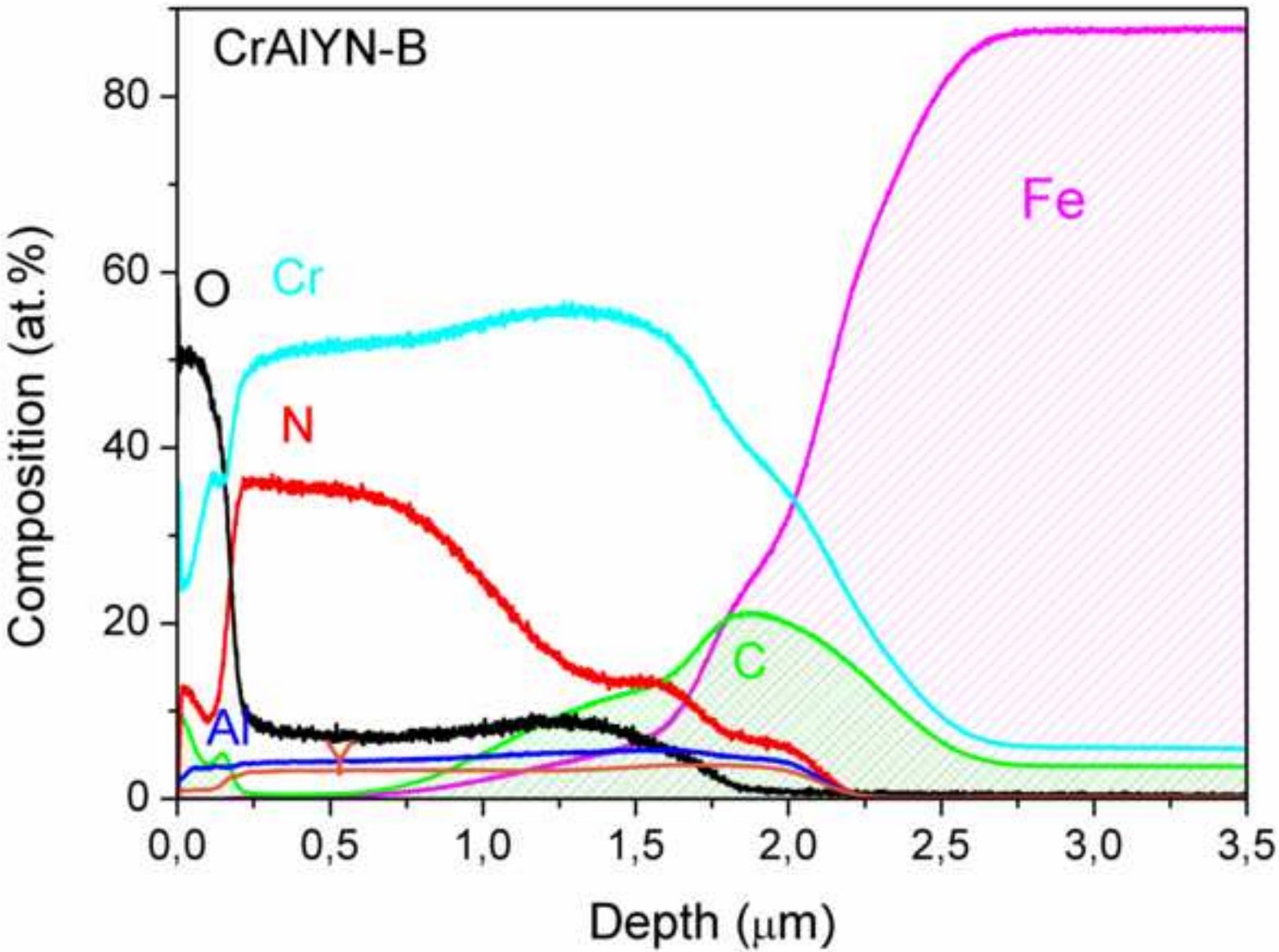

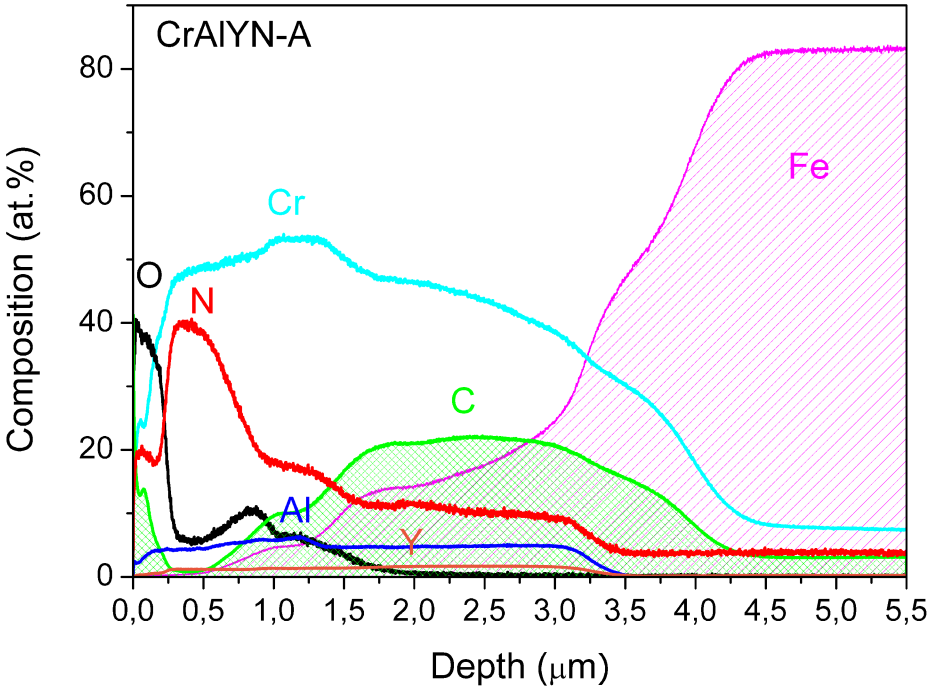
CrAlYN-A
Composition (at.%)
Depth (μm)
Cr
Fe
O
N
C
Al
Y
0
20
40
60
80
0,0
0,5
1,0
1,5
2,0
2,5
3,0
3,5
4,0
4,5
5,0
5,5

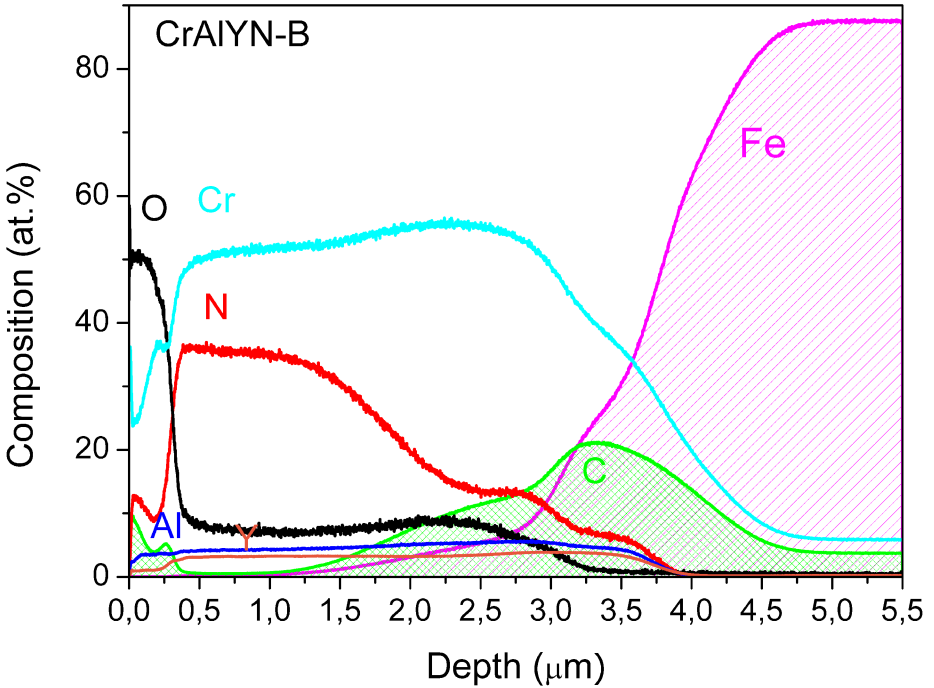
CrAlYN-B
Composition (at.%)
Depth (μm)
O
Cr
N
Al
Y
C
Fe
0
20
40
60
80
0,0
0,5
1,0
1,5
2,0
2,5
3,0
3,5
4,0
4,5
5,0
5,5

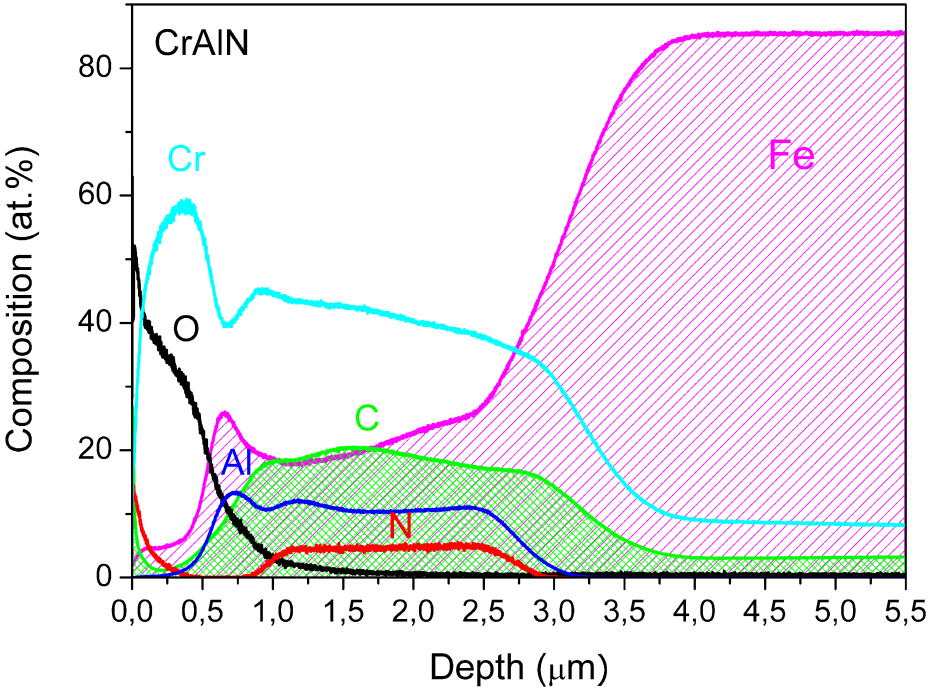
CrAlN
Cr
Fe
O
C
Al
N
Composition (at.%)
Depth (μm)
0
20
40
60
80
0,0
0,5
1,0
1,5
2,0
2,5
3,0
3,5
4,0
4,5
5,0
5,5